# Radiation-Free 3D Navigation and Vascular Reconstruction for Aortic Stent Graft Deployment

Fang Chen, Jia Liu, and Hongen Liao(✉)

Department of Biomedical Engineering, School of Medicine, Tsinghua University, Beijing, China
liao@tsinghua.edu.cn

**Abstract.** We propose a radiation-free three dimensional (3D) navigation and vasculature reconstruction method to reduce aortic stent graft deployment time and repeated exposures to high doses of X-ray radiation. 2D intraoperative US images are fused with 3D preoperative magnetic resonance (MR) image to provide intuitive 3D navigation for deployment of the stent-graft in the proposed system. On the other hand, calibrated 2D US images track catheter's tip and construct intraoperative 3D aortic model by combining segmented intravascular ultrasound (IVUS) images. The constructed 3D aortic models can quantitatively assess morphological characteristics of aortic to assist deployment of stent graft. This system was validated by using in vitro cardiac and aorta phantom. The mean target registration error of 2D US-3D MR registration was 2.70 mm and the average tracking error of position of IVUS catheter's tip was 1.12 mm. Accurate contours detection results in IVUS images were acquired. Meanwhile, Hausdorff distances are 0.78 mm and 0.59 mm for outer and inner contours, respectively; Dice coefficients are 90.21 % and 89.96 %. Experiment results demonstrate that our radiation-free navigation and 3D vasculature reconstruction method is promising for deployment of stent graft in vivo studies.

**Keywords:** Radiation-free 3D navigation · Intravascular ultrasound segmentation · Ultrasound tracking · Registration

## 1 Introduction

Placement of endovascular stent graft is the most common approach for treatment of acute aorta dissection and aneurysm [1]. In this treatment, a stent graft is inserted into aortic lesions by using a catheter through a dissected femoral artery. For accurate stent graft deployment, there are two critical factors: (1) morphological characteristics information of aorta especially calcification areas for determining the size of stent graft [2]; (2) intuitive relative position information between catheter and three dimensional (3D) cardiac structure for assisting stent graft placement. Stent graft placement is typically guided by fluoroscopic guidance with the use of X-ray contrast. However, fluoroscopic guidance has three distinct disadvantages. First, although fluoroscopy can visualize the catheter excellently, soft tissue structures are not easily visualized. Poor 2Dvisualization of aorta and surrounding anatomy causes incorrect placement of stent.


G. Zheng et al. (Eds.): MIAR 2016, LNCS 9805, pp. 59–71, 2016.
DOI: 10.1007/978-3-319-43775-0_6

Second, 2D X-ray fluoroscopic image can't provide quantitative analysis of the vessel's morphological characteristics [3]. Third, repeated injection of contrast agents influences the health of patient and clinical staff.

To provide intuitive 3D navigation images, Fagan *et al.* proposed a 3D vascular geometry visualization method with rotational angiographic images [4]. Hybrid imaging systems which combined magnetic resonance (MR) and X-ray fluoroscopic images, can realize 3D guidance in endovascular interventions [5]. These methods undoubtedly increase X-ray radiation or bring magnetic compatibility problem. Moreover, electromagnetic (EM) tracking system has been widely used to collect 3D position information of catheter for endovascular guidance [6]. 3D information of catheter is also combined with preoperative images [7]. However, the EM tracking method can't acquire intraoperative movement information of soft tissue and has limitation on accuracy due to the increased size of the EM sensor-attached catheter. Recently, intravascular ultrasound (IVUS) images have been used for in vivo analysis of plaque morphology [8]. IVUS imaging is more accurate to guide stent deployment than conventional angiography including X-ray and MR imaging, because of the relatively higher resolution [9]. The semi-automatic vessel 3D reconstruction method from IVUS video sequences is used to evaluate vessel pathologies [10]. However, this method can only be used for blood vessels with small curvatures and can't acquire catheter position information. A cardiovascular modeling method fusing the IVUS images and EM tracking system is proposed without the utilization of X-ray images [11]. This method provides only 3D model of blood vessel, without 3D structure around target aorta. Real-time 2D echocardiography is commonly used to guide correct stent deployment for aortic dissection because it provides superior diagnostic accuracy than angiography [12], but this method provides only 2D non-intuitive images. In summary, it is still a challenge to develop a navigation method, which provide not only morphological characteristics information of aortic but also 3D guidance image of surrounding soft tissue.

In this paper, we propose novel radiation-free 3D endovascular navigation and vascular reconstruction system for aortic stent grafts deployment. We implement real-time 2D ultrasound (US) image to provide intraoperative information of soft tissue and track catheter. This method can provide 3D navigation image of aorta and surrounding tissue without X-ray radiation by fusing intraoperative 2D US and operative 3D MR images. 3D model reconstruction of aorta is achieved by combining morphological characteristics information obtained from IVUS image with corresponding position of IVUS catheter tip from US image tracking.

## 2 Materials and Methods

### 2.1 Configuration of Radiation-Free 3D Navigation and Vascular Reconstruction System

The radiation-free 3D navigation and vascular reconstruction system consists of an US device, a 3D optical tracking system, a computer, and a catheter (Fig. 1). The US system is used to obtain images of the intraoperative surrounding tissue and catheter's tip. The 3D optical tracking system collects the pose of the US probe. In addition, the IVUS scanning probe is inserted into the aorta through a catheter. The collected

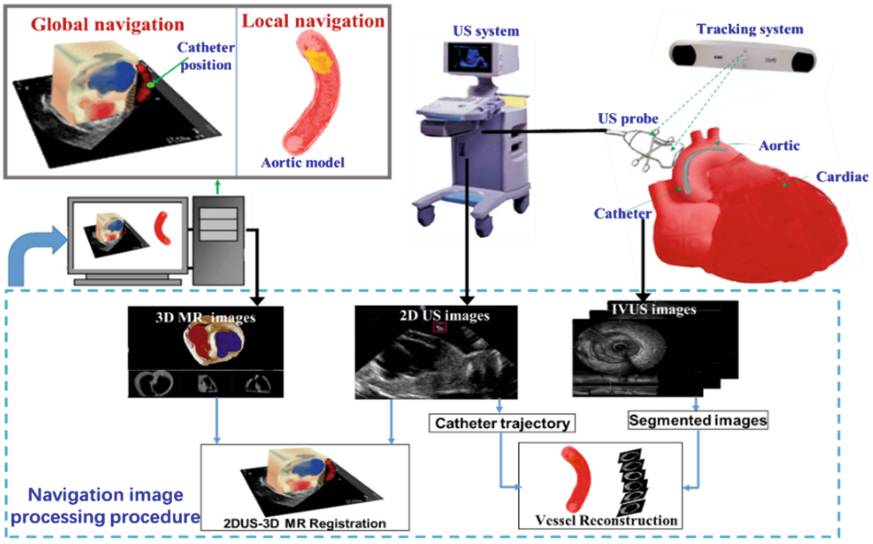


**Fig. 1.** System configuration of radiation-free 3D navigation and vascular reconstruction.

intraoperative US images, IVUS images and preoperative 3D MR images are combined and processed during image processing procedure. The image processing procedure mainly includes two parts: (1) 2D US-3D MR registration for 3D intuitive image information; (2) construction of 3D aorta model combining segmented IVUS images with catheter's trajectory from US images. Finally, the processed navigation image is displayed to guide aortic stent graft deployment.

## 2.2 Radiation-Free 3D Navigation and Vascular Reconstruction Workflow

The workflow of the proposed navigation and vascular reconstruction system is divided into two parts: preoperative processing and intraoperative processing.

**Preoperative Processing.**

- The preoperative high-quality 3D MR images of the cardiac and aorta are collected, which have a large field of view.
- Using the calibrated 3D US probe to collect 3D US image only one time in intraoperative preparatory stage.

**Intraoperative Processing.** Intraoperatively, the calibrated 2D US probe is implemented to collect real-time 2D US images. The US images contains both anatomical regions relating to the aorta and catheter tip.

- The 2D intraoperative US images are fused with 3D preoperative MR image to acquire intuitive 3D navigation information for stent graft deployment according to registration method in Sect. 2.3.

- The IVUS catheter's tip is tracked in US images and catheter's 3D trajectory is acquired according to Sect. 2.4.
- The IVUS images collected with IVUS catheter is semi-automatically segmented. Intraoperative 3D models of the aortic is reconstructed based on the segmented IVUS images and catheter's 3D trajectory (Sect. 2.5).
- Surgeons decide the size of stent graft according to morphological characteristics of 3D aorta especially plaque voxels and carry out aortic stent graft placement without radiation using intuitive 2D US-3D MR fusion image for navigation.

### 2.3 2D US-3D MR Image Registration Based on US Probes' Calibrations

Although US scan can obtain real-time imaging of soft tissue intraoperatively, the field of imaging and image quality are limited. Preoperative cardiac MR images have high image quality and a relatively large filed of imaging, which is seen as a practical clinical diagnosis tool [13]. But MR images lack real-time performance. So the combination of US and MR images is important to provide high-quality global 3D images. However, 2D US and 3D MR images have different image modality and dimensionality which makes 2D US-3D MR image registration become difficult. To address this problem, we apply a calibrated 3D US image to simplify traditional rigid 2D US-3D MR registration problem into two easy-achieved steps: 2D-3D US intra-modal registration and 3D US-3D MR intra-dimension registration. In our registration process, rigid registration transformation $T_{2DUS}^{3DMR}$ is calculated by

$$T_{2DUS}^{3DMR} = T_{2DUS}^{3DUS} * T_{3DUS}^{3DMR}, \tag{1}$$

where $T_{2DUS}^{3DUS}$ is transformation between intra-modal 2D and 3D US images, $T_{3DUS}^{3DMR}$ is registration transformation between intra-dimension 3D US and MR images.

In intraoperative preparatory stage, we employ a calibrated 3D US probe to collect 3D US image of the target organ only one time. The collected 3D US image has same dimension as MR image. And 3D US-3D MR preoperative registration is done manually using custom software (3D slicer) to acquire $T_{3DUS}^{3DMR}$.

In addition, crucial 2D-3D US intra-modal registration $T_{2DUS}^{3DUS}$ is achieved automatically by firstly using the 2D and 3D US probes' calibration results to get a near-optimal start value $\dot{T}_{2DUS}^{3DUS}$ and then doing intensity-based local registration adjustment to acquire final transformation $T_{2DUS}^{3DUS}$.

Firstly, the near-optimal start value of registration transformation $\dot{T}_{2DUS}^{3DUS}$ can be automatically calculated by

$$\dot{T}_{2DUS}^{3DUS} = T_{2DUS}^{TS} * (T_{3DUS}^{TS})^{-1} \tag{2}$$

Here

(i) $T_{2DUS}^{TS} = T_{2DPR}^{TS} * T_{2DUS}^{2DPR}$, where $T_{2DUS}^{2DPR}$ is 2D probe's calibration result (transformation between 2D US image coordinate and 2D US probe (2D PR) coordinate); $T_{2DPR}^{TS}$ transform from 2D probe coordinate (2D PR) to tracking system coordinate (TS) and it is recorded by external tracking system;

(ii) $T_{3DUS}^{TS} = T_{3DPR}^{TS} * T_{3DUS}^{3DPR}$, where $T_{3DUS}^{3DPR}$ is 3D probe's calibration result (transformation between 3D US image coordinate and 3D US probe coordinate (3D PR)); $T_{3\text{DPR}}^{TS}$ is transformation between 3D probe sensor coordinate (3D PR) to TS coordinate. $T_{3\text{DPR}}^{TS}$ is updated according to the pose of the 3D probe sensor and recorded by tracking system.

Secondly, with the acquired near-optimal start value of transformation $\dot{T}_{2DUS}^{3DUS}$, fast automatic intensity-based local registration adjustment is then employed for accurate registration. In local registration adjustment, we utilize mutual information (MI) as similarity metric. We use gradient ascent optimizer to find optimum value of MI metric and final rigid transformation $T_{2DUS}^{3DUS}$.

During our registration process, to solve used calibrations results of 2D and 3D US probes ($T_{2DUS}^{2\text{DPR}}$ and $T_{3DUS}^{3\text{DPR}}$), we design an applicative phantom (length: 26 cm, width: 12 cm, height: 28 cm) (Fig. 2). While performing calibration of 2D US probe, we use N-wire calibration phantom [14] with three N-wires (two types of N-wires) resembled on each layer (Fig. 2(a), (b)). By adding a wire to N-wire shape, we create an IXI-wire shape. For 3D US probe's calibration, we utilize an IXI-wire calibration phantom [15] with four IXI-wires (two types of IXI-wires) on four layers (Fig. 2(c), (d)). More detailed descriptions about calibration and registration procedure can be found in [16].

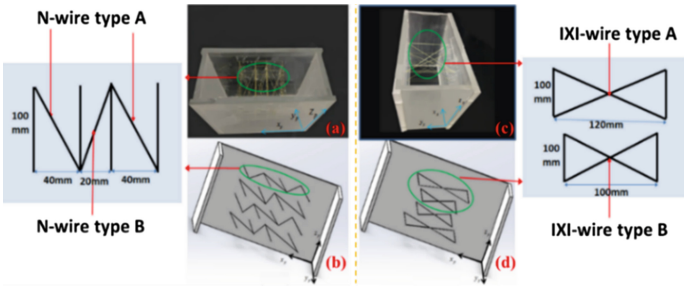


**Fig. 2.** Calibration phantoms; (a) real N-wire phantom; (b) CAD model of N-wire phantom; (c) real IXI-wire phantom;(d) CAD model of IXI-wire phantom.

## 2.4 Catheter Tip Tracking for Acquirement of 3D Trajectory

We use real-time 2D US images to collect intraoperative structural information including heart chambers and aorta, and simultaneously track the IVUS catheter's tip with US images. The catheter could be scanned in consecutive cross-sections with tracked US imaging. We apply a normalized correlation coefficient based template matching method to track the catheter tip in collected US images. Template matching algorithm is widely used for location of the signal and target object [17]. In 2D US images, the vessel's cross section is chosen as the region of interest (ROI) to be tracked. To identify the matching area, we try to find the maximum of matching metric which is defined as normalized correlation coefficient, by sliding the template image on the 2D

US images. The template size is set as 40 pixels × 40 pixels according to the size of the blood vessels in US images. Considering the amount of target movement between two adjacent frames, the ratio of template's size to search area's size is 5:1. By normalized correlation coefficient based template matching method, the cross-section of vessel is localized in each US image. Since the intensity of the catheter in US image is much higher than that of most of the speckle in the images, the position of IVUS's catheter can be easily acquired by using a threshold (the threshold value is set at 220 on 256 step scale). After thresholding, a morphological opening operation is performed to remove any spurious points. The tip of IVUS catheter is located in the last US image frame where the catheter can be detected. With 2D US probe's calibration result, the position of the IVUS catheter's tip under 2D US image coordinate can be transformed to the tracking system coordinates by using transform $T_{2DUS}^{TS}$ between 2D US image coordinate and tracking system. Once acquiring real-time positions of IVUS catheter's tip, the 3D trajectory of catheter is constructed.

## 2.5 IVUS Segmentation for 3D Aortic Reconstruction

3D aortic model can be reconstructed with segmented IVUS sequence and IVUS catheter trajectory. To achieve IVUS sequence segmentation, we apply a segmentation method which uses the information of IVUS sequence's dual views: the cross-sectional and longitudinal view. Figure 3 shows the segmentation and modeling workflow for collected IVUS sequence of the aorta with vascular plaque. In initialization stage, initial inner (lumen) and outer (media-adventitia) contours are manually delineated on six uniformly distributed longitudinal views of the IVUS sequence from $0^o$ to $360^o$. The initial contours in every cross-section of IVUS sequence are automatically acquired by a linear interpolation of six initial points from longitudinal views.

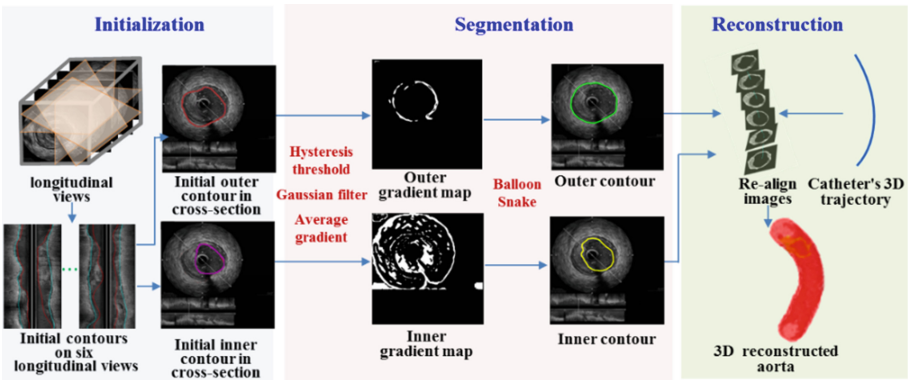


**Fig. 3.** The workflow of IVUS image segmentation and 3D vessel reconstruction.

In segmentation stage, the balloon snake model [18] is implemented to acquire final inner and outer borders guided by modified gradient maps. Deformable balloon snake model of contour detection applying gradient information as input is heavily

susceptible to image artifacts. So preprocessing is required to achieve gradient map with low noise for accurate detection. Firstly, we use the average gradient defined by Plissiti *et al.* [19] instead of standard gradient (difference between adjacent pixels) to avoid sharp changes in gradient and acquire expected smooth contour. Then, hysteresis thresholding and Gaussian filter are used to reduce unwanted gradient information in gradient map. The Gaussian filter is applied to reduce noise while maintaining edges and the hysteresis thresholding is utilized to remove extreme values unlikely to be involved in the detection of contours. The outer gradient map is modified with a hysteresis threshold, primarily to eliminate low gradients associated with the inner contour, and secondarily to eliminate high gradients associated with the catheter "shadow" artifact. For inner gradient map, it is modified with a hysteresis threshold, primarily to eliminate the gradients associated with the outer contour. And inner gradient map is further convolved with a radial Gaussian kernel centered at the average center of the initial inner contour to lower the effects of gradients far from the likely location of the inner contour. Finally, with acquired initial contours and gradient maps, we apply balloon snake to obtain borders in each frame with smoothness maintained.

In the reconstruction stage, with the use of automatic pullback device, constant pullback speed is assumed. Thus segmented IVUS frames can be realigned automatically at equidistant intervals on the acquired 3D catheter trajectory. For the distribution angles for the IVUS frames, image planes are positioned perpendicular to the catheter trajectory. After determining spatial location of each segmented IVUS image, 3D aortic model is reconstructed and is written as VTK file format. The final 3D aortic model is rendered in 3D Slicer.

## 3 Experiment and Results

The experiment platform was shown in Fig. 4. The 2D US images were collected by using US system (iU22 xMATRIX, Philips) with a 2D linear array probe (VL13-5, Philips). And 3D US image of the cardiac and aortic was collected just one time with 3D phased array probe (S5-1, Philips). Additionally, we used an optical tracking

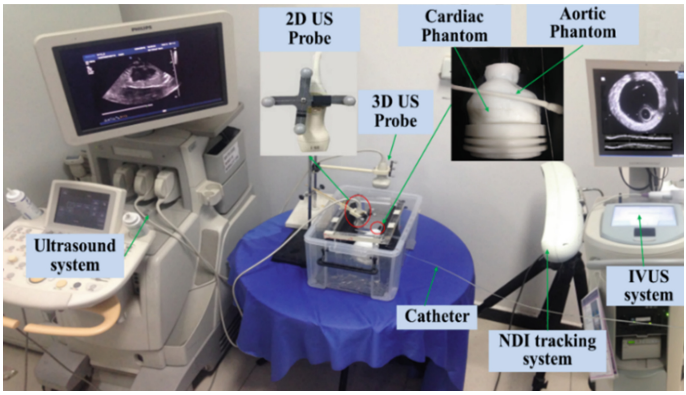


**Fig. 4.** The aortic and cardiac phantom experiment platform.

system (Polaris, Northern Digital Inc) to track US probes. The IVUS images were collected by using Boston Scientific Galaxy 2 system with a 40 MHz Atlantis SR IVUS probe at a pull-back speed of 0.5 mm per second. The simulated experiment used a MR compatible multi-modality heart phantom (SHELLEY Medical, USA), which contained left ventricular (LV) and right ventricular (RV) and an aortic phantom covered on it. Preoperative 3D MR images were collected with a MR scanner (Philips Achieva 3.0T TX) whose size was 480 × 480 × 300 voxels with resolution 0.4871 mm 0.4871 mm and slice thickness 1.6000 mm. The size of the 2D US images was 600 × 800 pixels with resolution 0.2382 mm × 0.2382 mm. IVUS images were 8-bits, 512 × 512 with in-frame resolution 0.0175 mm × 0.0175 mm.

### 3.1 Results of Probes' Calibration and 2DUS-3DMR Registration

**2D and 3D Probes' Calibration.** Calibration reproducibility (CR) error measured repeatability of a proposed probe calibration method when performed on a new set of images [14]. CR was the Euclidian distance between two calibration transformations ($T_{US}^{PRi}$ and $T_{US}^{PRj}$) of the same US image point $P^{US}$. CR error was usually calculated by

$$E^{CR} = \underset{i,j}{mean}\left\{\left\|T_{US}^{PRi} * P^{US} - T_{US}^{PRj} * P^{US}\right\|\right\} \tag{3}$$

During the evaluations of 2D and 3D probes' calibration, we both performed 8 calibration trials and used 10 images per trial, 80 datasets in total. The acquired CR error of 2D calibration was 0.61 mm and CR error of 3D calibration is 1.42 mm.

**2DUS-3DMR Image Registration.** Figure 5 showed the registration results of 2DUS-3DUS images, 3DUS-3DMR images and 2DUS-3DMR images during

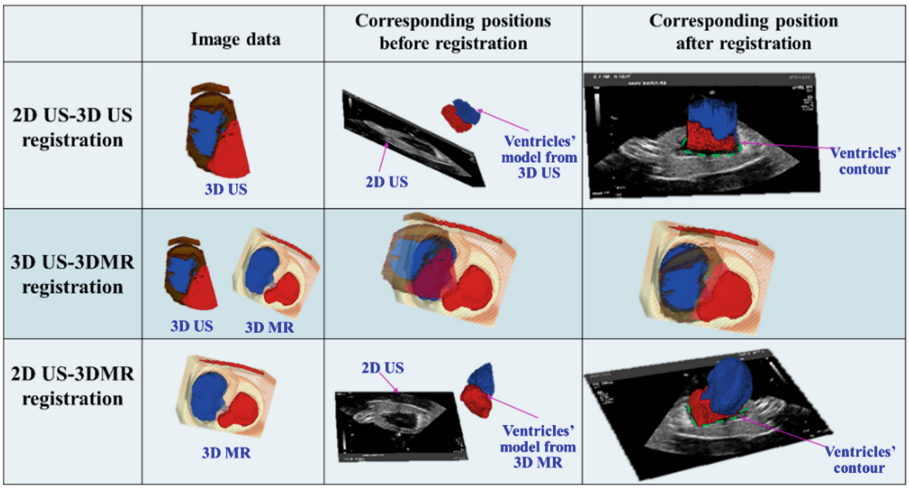


**Fig. 5.** Registration results of 2DUS-3DUS, 3DUS-3DMR and 2DUS-3DMR *(red volume is left ventricular model; blue volume is right ventricular model)*. (Color figure online)

registration process (see Fig. 5). The ventricle model from 3D US image was registered to corresponding ventricle's contour in 2D US images (see first row in Fig. 5), which verified the 2D-3D US registration based on US probes' calibration. The contours of the ventricle in 2D US and 3D MR images after registration achieved a good agreement (see third row in Fig. 5), which qualitatively demonstrated the proposed 2D US-3D MR image registration method was effective. In addition, 2D US-3D MR registration accuracy was further quantitatively evaluated by calculating the target registration error (TRE). 10 ventricle contour points in 2D US and corresponding ventricle contour points 3D MR model were manually delineated by expert surgeon to serve as fiducial marks. And TRE was defined as average Euclidean distance of these corresponding contour points. The registration result of 2D US and 3D MR image with a mean TRE of 2.70 mm (range 1.05 mm–3.67 mm) was acquired. On phantom experiment, our registration speed was about 11 s per frame in Matlab 2014 platform, which can be speeded up specifically by implementing the algorithm on C++ platform.

### 3.2 IVUS Segmentation and Catheter Tracking

**IVUS Image Segmentation.** The performance of the proposed IVUS segmentation method was evaluated using 200 IVUS images obtained from 5 sequences. These five IVUS sequences included one IVUS sequence of aorta phantom and four IVUS sequences of real patients. These sequences were collected by an IVUS expert from Navy PLA General Hospital. The detected inner and outer contours by proposed segmentation method were compared with manual segmentations by the anonymous IVUS expert to evaluate algorithm's accuracy. Figure 6 depicted our automatic segmentation examples of IVUS images along with manual segmentation. In addition, the performance of the segmentation method was quantified by using Hausdorff distance [20] and Dice index [21]. Table 1 provided the comparison results of our proposed

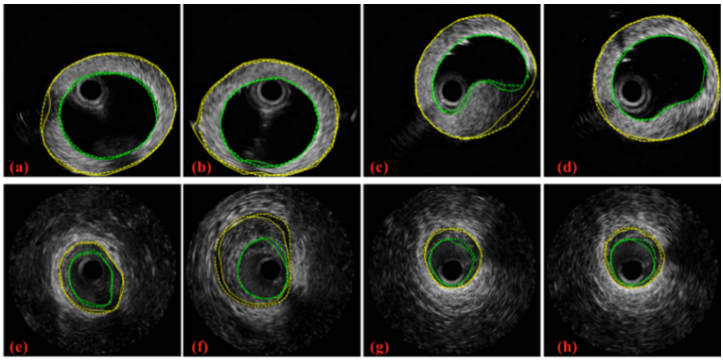


**Fig. 6.** Segmented contours of IVUS images ((a)–(d): IVUS images of vessel phantom; (e)–(h): IVUS images of real patients); yellow and green contours denote the outer and inner contours respectively. *(dotted lines denote detected contours by manual segmentation and full lines denote detected contours by proposed segmentation method, respectively).* (Color figure online)

**Table 1.** The segmentation results comparison between proposed method and manual tracing.

| Similarity and distance measurements | Outer contour | | Inner contour | |
|---|---|---|---|---|
| | Mean | SD | Mean | SD |
| Hausdorff distance | 0.78 mm | 0.24 mm | 0.59 mm | 0.31 mm |
| Dice index | 90.21 % | 7.53 % | 89.96 % | 5.91 % |

segmentation method and manual delineation. The mean Hausdorff distance and Dice index between automatic and manual segmentations were 0.59 mm and 89.96 % for inner contour detection. The Hausdorff distance and Dice index were 0.78 mm and 90.2 % for outer contour detection. The results validated that the proposed IVUS segmentation method was effective for detecting outer and inner contours.

**IVUS Catheter Tracking and Catheter's 3D Trajectory Reconstruction.** During the experiment, we inserted the IVUS catheter into aortic of the heart phantom and collected 2D US images to track the IVUS catheter. Catheter tracking result was shown in Fig. 7.

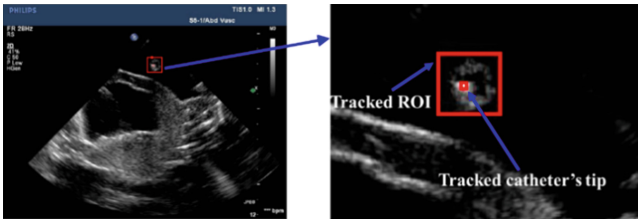


**Fig. 7.** Tracking results of IVUS catheter's tip. (Color figure online)

As shown in Fig. 7, the red box represents the tracked ROI (vessel's cross section). And the red point was the located tip of IVUS catheter (the brightest point of the ROI). During the experiments, we tracked catheter's tip in 100 US images and compared with manual delineative tip in each image to calculate tracking error. The tracking distance error was defined as the Euclidean distance between the manual delineative position and automatically tracked position. The acquired average tracking error was 1.12 mm with a standard deviation of 0.49 mm. After acquiring real time positions of IVUS catheter's tip, the 3D trajectory of the catheter was reconstructed under tracking system coordinate (Fig. 8). Figure 8 showed the 3D trajectory of the catheter by using automatic tracking results of catheter tip along with 3D catheter trajectory by manual tracking results.

The proposed radiation-free 3D navigation and vascular reconstruction system could provide the surgeon with hybrid navigation information for aortic stent graft deployment. There were three kinds of navigation information (see Fig. 9): (1) Global navigation. In global navigation, 3D MR cardiac structural image is registered with real time US images to provide an updated view of the surrounding tissue. And 3D position information of inserted catheter is overlaid on this 3D image; (2) Local navigation. In

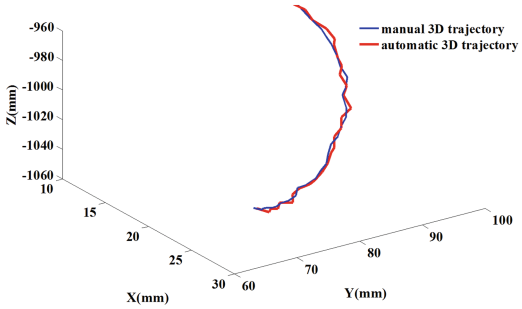


**Fig. 8.** 3D trajectory of the catheter in tracking system coordinate.

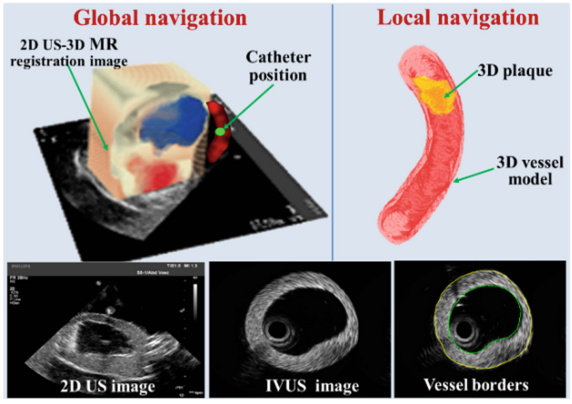


**Fig. 9.** Navigation information of radiation-free 3D navigation system.

local navigation, real intraoperative 3D model of aorta is reconstructed to provide morphological characteristics information of calcification; (3) Typical 2D views including 2D US images and segmented 2D IVUS images with the detected lumen and media-adventitia border.

## 4 Discussions and Conclusion

This paper presents a radiation-free 3D navigation and vascular reconstruction method for aortic stent graft deployment with the combination of IVUS, US and MR images. The proposed method can provide not only 3D real-time navigation images of cardiac and surrounding tissue, but also quantitative morphological characteristics of vessel to assist stent graft deployment without X-ray radiation. We have evaluated the proposed method on a realistic cardiac phantom experiment and the results validated the feasibility of the radiation-free 3D navigation method for guiding aortic stent graft deployment.

Our IVUS segmentation method is semi-automatic. In the future, to make segmentation method fully automatic, we will use automatic pixel classification method

such as machine learning, to acquire initial contours on longitudinal views of the IVUS sequence instead of manual delineated. Furthermore, in our phantom environment, the reality of our proposed catheter tip tracking method with US image is validated. To ensure that our tracking method is reliable for more complex image artifacts, we will combine more features' similarity criterion including histogram of oriented gradient feature and gray min average distance instead of single gray correlation coefficient. In our study, we have finished evaluations on a static heart phantom, and we will apply temporal alignment of US, MR and IVUS images through electrocardiograph (ECG) signals to solve the aorta's motion in different cardiac phases of beating heart. After solving these problems, our proposed radiation-free 3D navigation method will be used near-automatically to guide the aortic stent graft deployment on animal pig experiment.

The proposed radiation-free 3D navigation and vascular reconstruction method achieves the idea of combining global information of intuitive 3D images with local information of vessels' morphological characteristics to guide precise endovascular intervention. In this paper, the idea of global and local navigation combination is validated in aortic stent graft deployment guidance, and it may also work in other clinical applications of endovascular therapy like catheter intervention of oral cancers.

**Acknowledgments.** This study was supported in part by National Natural Science Foundation of China (Grant No. 81427803, 61361160417, 81271735), Grant-in-Aid of Project 985, and Beijing Municipal Science & Technology Commission (Z151100003915079). The Authors would like to thank Mr. Yigang Qiu from Department of Cardiology, Navy PLA General Hospital for assistance in acquiring IVUS data for this study.

## References

1. Dake, M.D., Kato, N., Mitchell, R.S., et al.: Endovascular stent–graft placement for the treatment of acute aortic dissection. New. Engl. J. Med. **340**(20), 1546–1552 (1999)
2. Timmins, L.H., Meyer, C.A., Moreno, M.R., et al.: Effects of stent design and atherosclerotic plaque composition on arterial wall biomechanics. J. Endovasc. Ther. **15** (6), 643–654 (2008)
3. Vykoukal, D., Chinnadurai, P., Davies, M.G.: Cardiovascular imaging, navigation and intervention: hybrid imaging and therapeutics. In: Garbey, M., Bass, B.L., Berceli, S., Collet, C., Cerveri, P. (eds.) Computational Surgery and Dual Training, pp. 125–148. Springer, New York (2014)
4. Fagan, T., Kay, J., Carroll, J., et al.: 3-D guidance of complex pulmonary artery stent placement using reconstructed rotational angiography with live overlay. Cathet. Cardio. Interv. **79**(3), 414–421 (2012)
5. Rhode, K.S., Sermesant, M., Brogan, D., et al.: A system for real-time XMR guided cardiovascular intervention. IEEE Trans. Med. Imaging **24**(11), 1428–1440 (2005)
6. Abi-Jaoudeh, N., Glossop, N., Dake, M., et al.: Electromagnetic navigation for thoracic aortic stent-graft deployment: a pilot study in swine. J. Vasc. Interv. Radiol. **21**(6), 888–895 (2010)

7. De Lambert, A., Esneault, S., Lucas, A., et al.: Electromagnetic tracking for registration and navigation in endovascular aneurysm repair: a phantom study. Eur. J. Vasc. Endovasc. **43** (6), 684–689 (2012)
8. Nishimura, R.A., Edwards, W.D., et al.: Intravascular ultrasound imaging: in vitro validation and pathologic correlation. Am. Coil. Cardiol. **16**, 145–154 (1990)
9. Brodoefel, H., Burgstahler, C., et al.: Accuracy of dual-source CT in the characterisation of non-calcified plaque: use of a colour-coded analysis compared with virtual histology intravascular ultrasound. Br. J. Radiol. **82**, 805–812 (2009)
10. Sanz-Requena, R., Moratal, D., García-Sánchez, D.R., et al.: Automatic segmentation and 3D reconstruction of intravascular ultrasound images for a fast preliminar evaluation of vessel pathologies. Comput. Med. Imag. Graph **31**(2), 71–80 (2007)
11. Shi, C., Kojima, M., Tercero, C., et al.: Intravascular modeling and navigation for stent graft installation based on data fusion between intravascular ultrasound and electromagnetic tracking sensor. In: 2012 IEEE International Symposium on Micro-NanoMechatronics and Human Science (MHS), pp. 229–234 (2012)
12. Franke, A., Kuhl, H.P., et al.: Quantitative analysis of the morphology of secundum-type atrial septal defects and their dynamic change using transesophageal three-dimensional echocardiography. Circulation **96**, II323–II327 (1997)
13. Finn, J.P., Nael, K., Deshpande, V., et al.: Cardiac MR imaging: state of the technology 1. Radiology **241**(2), 338–354 (2006)
14. Lindseth, F., Tangen, G.A., Langø, T., et al.: Probe calibration for freehand 3-D ultrasound. Ultrasound Med. Biol. **29**(11), 1607–1623 (2003)
15. Bergmeir, C., Seitel, M., Frank, C., et al.: Comparing calibration approaches for 3D ultrasound probes. Int. J. Comput. Assist. Radiol. Surg. **4**(2), 203–213 (2009)
16. Chen, F., Liao, R., Liao, H.: Fast registration of intraoperative ultrasound and preoperative MR images based on calibrations of 2D and 3D ultrasound probes. In: Jaffray, D.A. (ed.) World Congress on Medical Physics and Biomedical Engineering, pp. 220–223. Springer, Toronto (2015)
17. Lewis, J.P.: Fast template matching. In: Vision Interface, pp. 15–19 (1995)
18. Kass, M., Witkin, A., Terzopoulos, D.: Snakes: active contour models. Int. J. Comput. Vis. **1** (4), 321–331 (1988)
19. Plissiti, M.E., Fotiadis, D.I., Michalis, L.K., et al.: An automated method for lumen and media-adventitia border detection in a sequence of IVUS frames. IEEE Trans. Inf. Technol. Biomed. **8**(2), 131–141 (2004)
20. Dice, L.R.: Measures of the amount of ecologic association between species. Ecology **26**(3), 297–302 (1945)
21. Huttenlocher, D.P., Klanderman, G.A., Rucklidge, W.J.: Comparing images using the Hausdorff distance. IEEE Trans. Pattern. Anal. Mach. Intell. **15**(9), 850–863 (1993)